Glass formation in mechanically alloyed Fe-based systems

Article *in* Functional Materials Letters · December 2009

DOI: 10.1142/S1793604709000727

2 authors:

C. Suryanarayana
University of Central Florida
331 PUBLICATIONS **11,878** CITATIONS
SEE PROFILE

Satyajeet Sharma
Oerlikon
7 PUBLICATIONS **111** CITATIONS
SEE PROFILE

Functional Materials Letters
Vol. 2, No. 4 (2009) 147–155

World Scientific
www.worldscientific.com

GLASS FORMATION IN MECHANICALLY ALLOYED Fe-BASED SYSTEMS

C. SURYANARAYANA* and SATYAJEET SHARMA†
Department of Mechanical, Materials and Aerospace Engineering
University of Central Florida, Orlando, Florida 32816-2450, USA
**csuryana@mail.ucf.edu*

Received 15 May 2009; Revised 30 September 2009

Rapid solidification processing of metallic melts has been traditionally employed to synthesize metallic glasses in several alloy systems. However, in recent years, solid-state processing methods, and more specifically, mechanical alloying, have become popular methods to synthesize glassy phases in metallic alloy systems. Although a large number of criteria have been developed to identify alloy compositions that can be solidified into the glassy state, very few attempts have been made to predict the glass-forming ability by solid-state processing methods. To evaluate if some clear criteria could be developed to predict glass formation by solid-state processing methods and to understand the mechanism of glass formation, mechanical alloying of powder blends was conducted on several Fe-based alloy systems. Three different aspects of glass formation are specifically discussed in this paper. One is the development of a criterion for identifying glass-forming systems from phase diagram features, the second is the process of mechanical crystallization (formation of a crystalline phase on continued milling of the amorphous powders obtained by mechanical alloying), and the third is the novel phenomenon of lattice contraction during amorphization. It was shown that the conditions under which a glassy phase is formed by mechanical alloying are different from the solidification methods.

Keywords: Glass formation; mechanical alloying; glass-forming ability; mechanical crystallization; lattice contraction.

1. Introduction

Metallic glasses (or amorphous alloys) have interesting and useful physical, chemical, mechanical, and magnetic properties that make them attractive for different applications.[1–3] Since the 1960s,[4] metallic glasses, with a thickness of $< 50\,\mu$m, were produced by rapid solidification processing (RSP) at high solidification rates of $> 10^5$ K/s in the form of flakes, wires, ribbons or powders. The last twenty years have witnessed the development of bulk metallic glasses with section thicknesses larger than 10 to 20 mm and at solidification rates of 1 to 100 K/s.[5–8] This was possible by increasing the number of components in the alloy system and choosing the appropriate compositions. However, for the successful synthesis of new and improved compositions that could be cast into still thicker sections for exploitation in industrial applications, prediction of the glass-forming ability (GFA) of alloys, especially in commercially important alloy systems should be made possible.

The ability of an alloy to form a glassy phase on solidification has been termed GFA. Glass formation in an alloy system is a complex phenomenon and therefore it is difficult to predict the GFA of alloys. In spite of this, a large number of criteria have been proposed in recent years. The most important among these are the critical cooling rate for glass formation (or the maximum section thickness), reduced glass transition temperature, T_{rg} (defined as $T_{rg} = T_g/T_l$, where T_g and T_l represent the glass transition and liquidus temperatures of the alloy, respectively), large atomic size difference between the constituent atoms, and the γ parameter[9] defined as $\gamma = T_{x1}/(T_g + T_l)$, where T_{x1} is the first crystallization temperature of the glassy phase. All the different criteria have been critically evaluated recently and it was shown that most of them have approximately similar predictive capabilities.[10]

Majority of the above criteria have been proposed to explain glass formation by (slow or rapid) solidification from the liquid state. But, a number of solid-state processing methods are also available to produce amorphous phases; the most important being mechanical alloying or milling. However, it is not clear whether the conditions and the mechanism for glass formation are similar between the liquid-state

*Corresponding Author.
†Present address: Sulzer Metco (US), Inc., Westbury, NY 11590, USA.

and solid-state processed alloys; the major objectives of this investigation.

Mechanical alloying (MA) is a solid-state powder processing method that involves repeated cold welding, fracturing, and rewelding of powder particles in a high energy ball mill. It has been shown that this technique is capable of producing equilibrium and supersaturated solid solutions, intermetallic phases, nanostructured materials, and metallic glasses.[11,12] MA has been shown to produce amorphous phases more easily and in a much wider composition range than by solidification methods. Further, an important advantage of MA as applied to bulk metallic glasses is that the limitation of section thickness noted in solidification methods can be easily overcome. This is because the amorphous powders produced by MA could be easily consolidated into bulk shapes of any size and shape in the supercooled liquid region.[13]

2. Experimental Procedure

Blended elemental (BE) pure metal powders (of $> 99.9\%$ purity) were weighed out corresponding to the generic composition of $Fe_{42}X_{28}Zr_{10}B_{20}$ (where the subscripts represent the composition of the alloy in atomic percentage and X = Al, Co, Ge, Mn, Ni, or Sn). Other alloying elements such as Nb and C have also been added to the above composition in some investigations. Additionally, a multicomponent Fe-based alloy composition has also been investigated. MA was carried out in a SPEX CertiPrep 8000 D shaker mill. For each experiment, 10 g of the blended elemental powder mix and 100 g of stainless steel balls were loaded into the milling container, thus maintaining a ball-to-powder weight ratio of 10:1 during milling. The ball sizes used were of 2 mm and 4 mm diameter respectively, to achieve better milling conditions. About 1 wt.% of stearic acid was added as a process control agent to prevent severe agglomeration of the powder to the vial walls and/or the grinding medium. The weighing, blending, loading and unloading of the powders were carried out inside a glove box with a controlled atmosphere of argon gas, so as to minimize powder contamination.

The phase evolution during milling was monitored by X-ray diffraction (XRD) using a Rigaku X-ray diffractometer with CuK_α radiation ($\lambda = 0.15406$ nm) at 40 kV and 35 mA settings. The XRD patterns were recorded in the 2θ range of 30 to 90°. To check the reliability of peak positions, the XRD unit was calibrated with a standard material (pure quartz), and occasionally the reference material was also mixed with the milled powder. The peak positions in the XRD patterns were determined by fitting the peaks to a Gaussian profile. Identification of the phases present and calculation of the lattice parameter were done using standard XRD procedures.[14] The GFA was quantified in terms of the milling time required for the glassy phase to form from the blended elemental powder mix; the shorter the milling time for amorphization, the higher is the GFA. Transmission electron microscopy studies were also conducted on selected milled powder samples.

3. Results and Discussion

The results of the present study are described in three groups. The first is on the criteria for glass formation, the second on mechanical crystallization, and the third on the mechanism of glass formation.

3.1. *Criteria for glass formation*

A large number of criteria have been proposed to explain glass formation in alloys but most of these criteria have been developed for glassy phases in alloys produced by solidification methods. For example, the criterion of negative heat of mixing between the constituent elements is necessary for alloying to take place in the liquid state and quenching from the liquid state has then been found to facilitate glass formation. However, in the case of MA, a large number of alloy systems with constituent elements having a positive heat of mixing have been found to alloy and even form amorphous phases.[15] Thus, there exists an important difference in the requirements for formation of amorphous phases between the two processing techniques. This is because MA is carried out at or near room temperature. Since no liquid phase is involved and at the temperature of operation the atomic mobility is very low, restrictions of equilibrium phase diagrams do not apply to alloys processed by MA.

Figure 1 shows the XRD patterns of the blended elemental powder mixture of $Fe_{42}Ni_{28}Zr_{10}B_{20}$ as a function of milling time. While all the expected diffraction peaks of Fe, Ni, and Zr are seen in the as-blended powder, peaks from boron are not seen probably because of its low scattering factor. On milling the powder mix for 10 h, it is noted that amorphization had occurred, as evidenced by the presence of a broad diffuse peak centered at the $(110)_{Fe}$ position. On further milling (for 40 h approx.), however, this diffuse peak became sharp, and additional low-intensity peaks started appearing. This process, referred to here as mechanical crystallization, will be discussed later in some detail.

Milling of powders of other compositions with X = Al, Co, Ge, Mn, and Sn gave different results. For example, an amorphous phase did not form in the systems containing Co, Mn, and Sn, but formed in alloys with Al and Ge.[16] Electron microscopy studies confirmed the presence of the amorphous phase in these alloy systems.[17]

The phase formation sequence in all the six powder blends, as a function of milling time, can be broadly

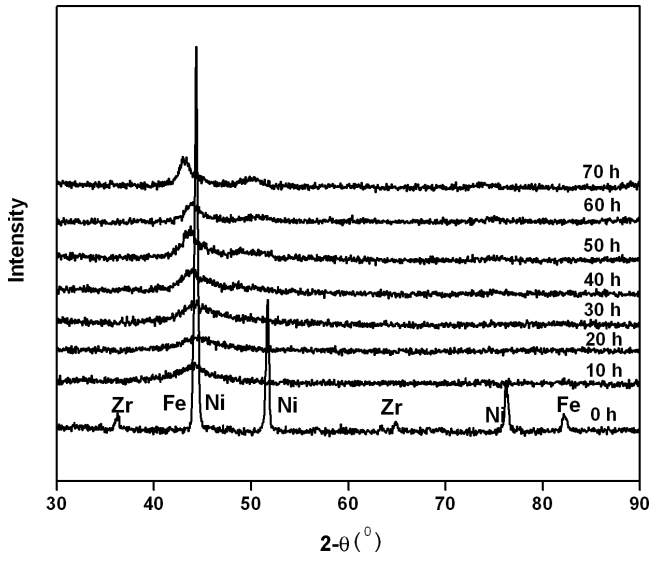

Fig. 1. XRD patterns of blended elemental powder mix of $Fe_{42}X_{28}Zr_{10}B_{20}$ (X = Ni) as a function of milling time. Note that the amorphous phase has started to form on milling for about 10 h and its formation was completed by 20 h. While the amorphous phase was stable up to about 30 to 40 h, milling beyond this time resulted in mechanical crystallization of the amorphous powder. Similar results were obtained in alloys containing X = Al or Ge.

categorized into three groups as follows:

(i) BE Powder → Intermetallics → Solid Solution
Examples: Mn- and Sn-containing systems
(ii) BE Powder → Solid Solution
Example: Co-containing system
(iii) BE Powder → Intermetallics → Amorphous Phase → (Mechanical) Crystallization
Examples: Al-, Ge-, and Ni-containing systems

The time of milling at which the amorphous phase had formed is termed the time of amorphization, which can be considered as a measure of the GFA of the alloy. This time of amorphization (and GFA) is different for different powder blends. Even though the XRD patterns are presented usually at intervals of 10 h, X-ray analysis was also conducted more frequently, whenever necessary. Table 1 lists the times required for amorphization in different alloy systems.

Reasons for the formation of an amorphous phase in some alloy systems and its absence in the others are obviously related to the GFA of the different alloys. However, since we are dealing here with the occurrence of the amorphous phase by the process of MA, we will not be able to relate the GFA to the properties of the liquid phase in these alloy systems. Therefore, we turned our attention to the features of the equilibrium phase diagrams. Since quaternary phase diagrams were not available for most of the alloy systems, the focus was on the binary phase diagrams of the constituent elements. All the X elements form at least one intermetallic phase with Zr, while with Fe and B, some of the X elements form intermetallics and

Table 1. Summary of the results of amorphization in the $Fe_{42}X_{28}Zr_{10}B_{20}$ (where X = Al, Co, Ge, Mn, Ni, or Sn) systems. The number of intermetallics in the constituent binary alloy systems with X (i.e., Zr-X, Fe-X, and B-X) is also listed.

X	Number of intermetallics between X and other elements			Total number of intermetallics	Milling time required for amorphization (h)
	X and Zr	X and Fe	X and B		
Al	8	5	2	15	10
Co	5	Nil	3	8	No amorphization
Ge	5	5	Nil	10	10
Mn	1	Nil	5	6	No amorphization
Ni	7	1	4	12	20
Sn	3	2	Nil	5	No amorphization

with others they do not. Table 1 also lists the number of intermetallic phases present in the constituent binary equilibrium phase diagrams.[18]

Two important conclusions can be drawn from a cursory observation of this Table. First, it is clear that amorphization is observed only in those alloy systems that contain a large number of intermetallic phases, i.e., a minimum of 10. Second, the higher the GFA, the larger the number of intermetallics. For example, the time required for amorphization is 10 h when the total number of intermetallics present is 15, while it is 20 h for 12 intermetallics. Note, however, that when the total number of intermetallics is only 10 (with the Ge-containing alloy), the time required for amorphization is only 10 h. But, this is a special case because Ge is a semi-metal with strong directional bonds. Thus, it becomes easier to amorphize alloys containing Ge (or other semi metals). From a critical analysis of the constituent binary phase diagrams, it also becomes clear that when the phase diagrams contain extensive solid solutions, it will be very difficult to amorphize them.

Amorphization by MA occurs when the free energy of the crystalline phase, G_C is higher than that of the hypothetical amorphous phase, G_A, i.e., $G_C > G_A$.[19] A crystalline phase normally has a lower free energy than the amorphous phase. But, its free energy can be increased by introducing a variety of crystal defects such as dislocations, grain boundaries, stacking faults, etc. If an intermetallic has formed, then additional energy can be introduced by disordering the crystal lattice. By this approach, it is then possible to obtain a situation when $G_C + G_D > G_A$, where G_D is the free energy increase due to introduction of defects.

The magnitude of energy increase is different for different types of defects. As an example, increasing the dislocation density to $10^{16}/m^2$ increases the free energy by about 1 kJ/mol, while decreasing the grain size down to 1 nm increases the free energy by about 10 kJ/mol.[20] On the other hand, disordering of the ordered intermetallic compound lattice can increase the free energy by as much as 15–20 kJ/mol.[21] Thus, it becomes easier to significantly raise the free energy of the crystalline

intermetallic phase by disordering the lattice either by destroying the long-range order or introducing non-stoichiometry into the system. That is, significant increase in free energy can be obtained by MA of intermetallic powders and not in the case of solid solution alloys. XRD patterns of the alloys transforming into the amorphous state indeed showed that intermetallic phases had formed in the early stages of milling. Thus, the energy increase of the MA system could be related to the disordering of the intermetallic phase through heavy mechanical deformation, shown possible earlier by heavy deformation.[22]

Phase diagram features have been used to predict glass formation by RSP and other methods as well. For example, since alloys with high T_{rg} values are known to be good glass formers, and alloys in the vicinity of deep eutectics exhibit high T_{rg} values, deep-eutectic alloy compositions have been shown to exhibit high GFA.[23] Further, elemental solids exhibiting a large number of polymorphic phases have been shown to exhibit higher GFA than elements that do not have a large number of polymorphs.[24] In contrast, amorphous phases are obtained mostly around equiatomic compositions by the MA methods. Also, the composition range for amorphous phase formation is much wider in alloys produced by MA than in those obtained by RSP.[11,12] Difficulty in amorphization has been observed with RSP in alloys having melting maxima, too many peritectic reactions, high-temperature eutectics and also alloys having positive heats of mixing. However, amorphization has been observed in most of these cases by MA.[11,12] Further, it was observed that it is not possible to transform very dilute alloys (with low concentration of solute atoms) to the amorphous state by MA methods,[25] whereas solute contents of as low as 9 at.% were found sufficient for glass formation in Fe-Zr and Co-Zr alloy systems by RSP methods.[26] Thus, even though phase diagrams are useful guidelines in choosing alloy compositions for easy glass formation by both methods, the features to look for appear to be quite different for the RSP and MA methods. It is just fortuitous that some alloy compositions can be amorphized by both the methods.

3.2. *Mechanical crystallization*

It was briefly mentioned in the previous section that an amorphous phase transforms into a crystalline phase on continued milling, and that this phenomenon was referred to as mechanical crystallization. This is a very unusual process and has a lot of potential applications in alloy design approaches since it will be possible to produce the alloy in either a fully amorphous, amorphous+nanocrystalline composite, or a completely crystalline state with different grain sizes, depending upon the time of milling or the temperature and time of annealing of the amorphous alloy.

Figure 2(a) shows the XRD patterns of the blended elemental powder of the composition $Fe_{42}Ge_{28}Zr_{10}B_{20}$ mechanically milled for 10 and 60 h. One may note the significant change in the XRD patterns. While the pattern at 10 h of milling clearly shows the presence of an amorphous phase, the pattern at 60 h shows the presence of a crystalline phase,

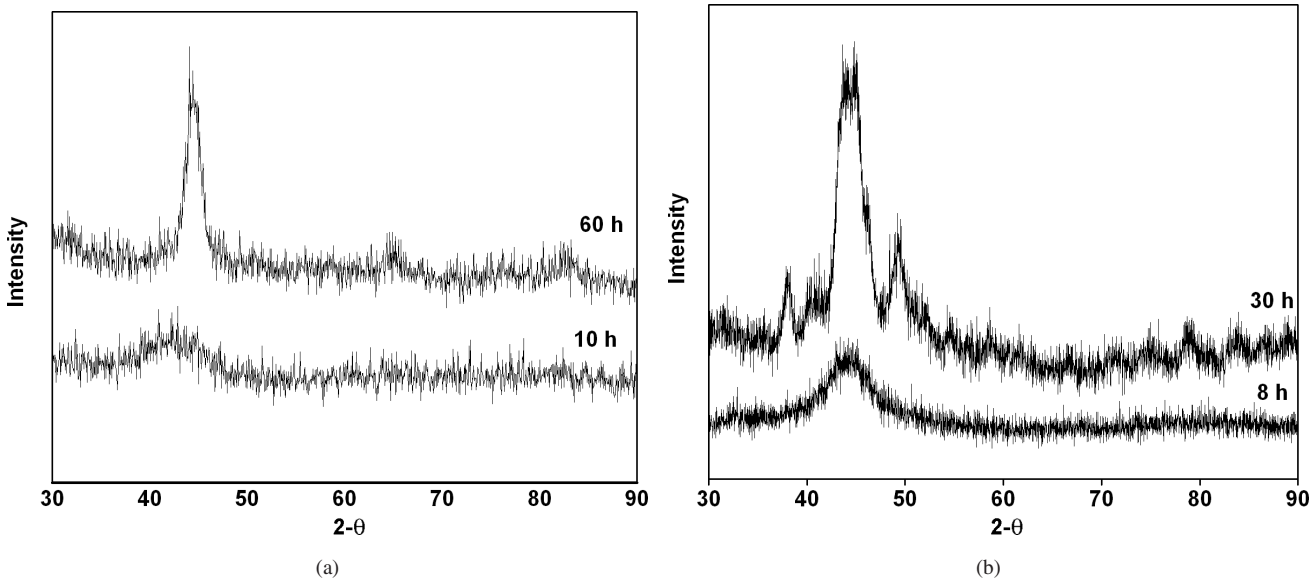

Fig. 2. (a) XRD patterns of the $Fe_{42}Ge_{28}Zr_{10}B_{20}$ powder mix milled for 10 and 60 h. While the powder mix milled for 10 h clearly shows the presence of an amorphous phase, the powder milled for 60 h shows mechanical crystallization. Also note the shift in the diffraction maximum of the amorphous phase (corresponding to the 110 peak of the α-Fe solid solution) from the clear 110 peak in the crystalline phase at 60 h. This significant shift is due to the change in the composition of the phase and therefore the lattice parameter. (b) XRD patterns of the $Fe_{42}Ni_{28}Zr_{10}C_{10}B_{10}$ powder blend milled for 8 and 30 h. The powder milled for 8 h is fully amorphous but the powder milled for 30 h contains a mixture of the amorphous and crystalline phases, a result of mechanical crystallization. A slight difference in the diffraction maximum of the amorphous phase and the $(110)_{Fe}$ peak position in the 30 h pattern is also noted.

superimposed over the broad and diffuse halo, characteristic of the amorphous phase. By analyzing the sharp diffraction peaks, it was possible to establish that the crystalline phase corresponds to the BCC structure with the lattice parameter $a = 0.2878$ nm, suggesting that this is an α-Fe solid solution containing the solute elements present in the blend. Primary crystallization of metallic glasses produced by RSP methods was shown to produce a crystalline solid solution phase coexisting with an amorphous phase, which has a composition different from that of the initial amorphous phase.[27] Thus, formation of the α-Fe phase in our MA powder may be interpreted to be a result of primary crystallization occurring in the amorphous alloy.

Figure 2(b) shows the XRD patterns of the $Fe_{42}Ni_{28}Zr_{10}C_{10}B_{10}$ powder blend milled for 8 and 30 h. Similar to Fig. 2(a), the powder milled for 8 h is fully amorphous and the same powder milled for 30 h shows the presence of sharp crystalline peaks superimposed over the amorphous phase. However, the important difference between Fig. 2(a) and Fig. 2(b) is that while the crystalline phase is the α-Fe solid solution in Fig. 2(a), it is a mixture of crystalline phases in Fig. 2(b). Thus, the sequence of phase formation in these powders during milling is that the blended elemental powder first forms intermetallic phases, then an amorphous phase, and eventually mechanical crystallization occurs resulting in the formation of crystalline phase(s).

Mechanical crystallization processes have also been observed in other alloy systems that formed the amorphous phase on MA, e.g., $Fe_{42}X_{28}Zr_{10}B_{20}$ systems with X = Al or Ni. But, it is not always the α-Fe solid solution phase that forms during mechanical crystallization of the Fe-based alloys. Sometimes, it has been noted that more than one phase forms simultaneously from the amorphous phase, i.e., as in Fig. 2(b) in the Fe-Ni-Zr-C-B system.[17] Eutectic crystallization is also reported to occur in several glassy alloys synthesized by melt spinning.[27]

It is now becoming apparent that this phenomenon of mechanical crystallization is not as rare as it was once thought to be.[28] There can be many reasons for the formation of a crystalline phase after the formation of an amorphous phase during MA. The important factors could be (i) rise in temperature to a level above that of the crystallization temperature of the amorphous alloy, (ii) powder contamination due to which a stable crystalline impurity phase forms, (iii) phenomenon of inverse melting, and (iv) basic thermodynamic considerations.

The maximum temperature rise during MA is about 200 K,[11,12] which is not sufficient for crystallization of the amorphous phase in Fe-based alloy systems. A crystalline phase may also form due to powder contamination such as in reactive metals.[11,12,29] If such a contaminant phase was formed, it will not revert to the equilibrium phases on annealing it. However, the equilibrium phases have formed in all the powders in the present investigation on annealing them for a sufficiently long time. Therefore, it can be concluded that the crystalline phase formed is not due to contamination. Requirements for the occurrence of inverse melting[30] are also not met in these alloys and therefore it could be concluded that the basic thermodynamic stabilities of the different phases under the conditions of milling are responsible for this process of mechanical crystallization. This can be further explained with reference to a free energy vs composition diagram.

Figure 3 is a schematic diagram showing the variation of free energy with composition for the Fe-based alloy systems investigated here. The possible phase constitution in the system is (a) blended elemental (BE) powder mixture, (b) α-Fe, the solid solution of all the alloying elements in Fe, (c) an amorphous phase, (d) intermetallic phases, and (e) different combinations of these phases. The stability of any phase will be determined by its relative position in the free energy plot – the lower the free energy the more stable the phase is. Since it is possible to have a large number of intermetallic phases in this multicomponent system, and it is difficult to indicate each of them separately, for simplicity, all of them are grouped together as "Intermetallics". We will now consider the relative stabilities of the different competing phases in the $Fe_{42}X_{28}Zr_{10}B_{20}$ system. For our discussions here, we will consider all the solute elements together, which make up to 58 at.%, as "solute".

The free energy of the BE powder mixture is indicated by point "1", which represents the point of intersection of the

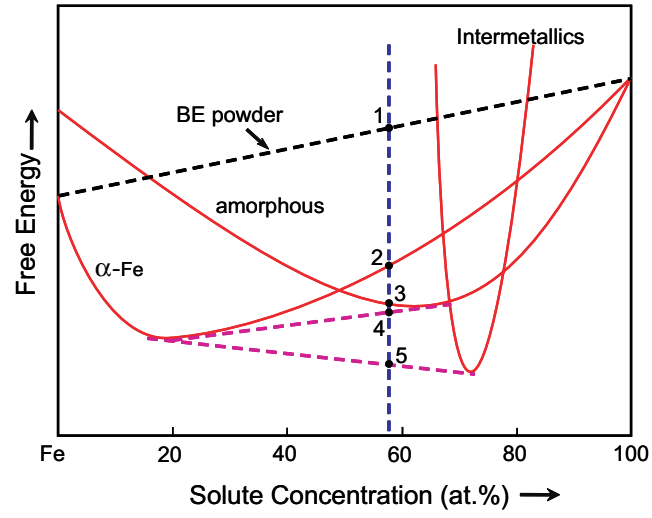

Fig. 3. Hypothetical free energy vs composition diagram to explain the mechanism of mechanical crystallization. Point "1" represents the free energy of the blended elemental powders. Point "2" and point "3" represent formation of the α-Fe solid solution of all the alloying elements in Fe, formation of the homogeneous amorphous phase respectively, and point "4" a mixture of the amorphous phase with a different solute content (amorphous) than at "3" and the solid solution α-Fe, and point "5" is for the equilibrium situation when the equilibrium solid solution and intermetallics coexist.

composition vertical with the line joining the free energies of pure Fe and the "solute". On milling this powder, a solid solution phase containing all the solute elements in Fe (or a mixture of intermetallics and a solid solution, in some cases) is seen to form and its free energy is indicated by point "2". The solid solution forms because it has a lower free energy than the BE powder mixture. Since MA introduces a variety of crystal defects such as dislocations, vacancies, stacking faults, and grain boundaries, the crystalline phases in the milled powders will contain excess energy. This energy will continue to increase with milling time and reach a point which is above that of the metastable amorphous phase. Thus, the amorphous phase gets stabilized (point "3"). On primary crystallization of the amorphous phase, the new constitution will be a mixture of the α-Fe solid solution or intermetallics and the amorphous phase, which now has a composition different from the original amorphous phase. Further, the new solid solution phase also has a composition different from the original α-Fe phase. The free energy of the mixture of this solid solution and the amorphous phases, indicated by "point 4", will have a free energy lower than that of the amorphous phase. The equilibrium mixture of the α-Fe solid solution and "intermetallics" will have the lowest free energy of all the phase mixtures, as indicated by point "5" in the figure. It may be noted that the process of mechanical crystallization is unique to the MA process and can only be achieved on milling the amorphous powder.

3.3. *Lattice contraction during amorphization*

As mentioned earlier, amorphous phases have been produced in several Fe-based alloys by MA. Based on a recent report that addition of an alloying element with a positive heat of mixing with a constituent element in a given alloy system improves the GFA and also the plasticity of the inherently brittle bulk glassy alloy,[31] we decided to investigate whether the GFA can be improved in the MA-processed amorphous phases. Indeed, this should be more favorable during amorphization by the MA methods, since MA of immiscible metals has been known to form amorphous phases.[11,15]

The element Nb was chosen because it exhibits a positive heat of mixing with Zr (+17 kJ/mol).[32] Additionally, Nb has an atomic diameter 0.2936 nm, substantially larger than that of Fe (0.2482 nm) and Ni (0.2492 nm), but smaller than that of Zr (0.3186 nm). Accordingly, we prepared BE powder mixtures of $Fe_{42}Ni_{28}Zr_{10-x}Nb_xB_{20}$ with $x = 1, 2, 4$, and 6 at.% Nb. Milling of these powders led to the observation of two important features. The first was that the ease of glass formation was different depending on the Nb content. The highest GFA was achieved in the powder blend with 2 at.% Nb. The second, and more interesting observation was that lattice contraction was observed at the time of amorphization.

Table 2. Time required for amorphization in the $Fe_{42}Ni_{28}Zr_{10-x}Nb_xB_{20}$ powder mix.

At.% Nb	Time for amorphization (h)
0	20
1	10
2	8
4	10
6	15

Table 2 lists the time necessary for amorphization in the $Fe_{42}Ni_{28}Zr_{10-x}Nb_xB_{20}$ powder mix as a function of Nb content. It may be noted that the time decreases from 20 h in the Nb-free alloy to the minimum value of about 8 h, in the alloy with $x = 2$, suggesting that the GFA was highest at this Nb content. Reduced milling times were observed for amorphization in the other powder blends with $x = 1, 4$, and 6 at.% Nb and the times required for amorphization were different at different Nb contents.

The position of the broad diffuse peak, representing the amorphous phase in the XRD patterns, was measured. To get a better appreciation of the peak shifts, the X-ray broad peaks were fitted to a Gaussian profile. Figure 4 shows the variation of the 2θ values as a function of milling time and for different Nb contents. It is clear from this figure that the position of the $(110)_{Fe}$ peak has shifted with milling time in all the cases, although apparently not in a consistent manner. In the initial stages of milling, the 2θ value decreased suggesting that the lattice parameter has increased, due to formation of an α-Fe solid solution. Since all the substitutional solute elements have an atomic size larger than that of Fe, and B dissolves interstitially, the lattice is expected to dilate and therefore the 2θ value will decrease with milling time. But, with continued milling, this crystalline phase becomes destabilized resulting in the formation of an amorphous phase.

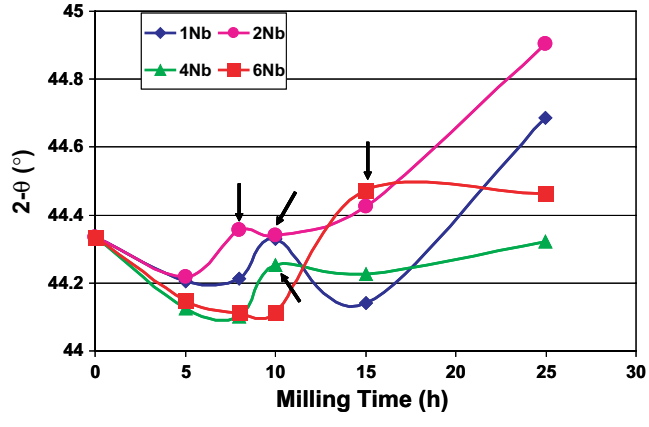

Fig. 4. Variation of the 2-θ values corresponding to the diffuse broad peak with milling time for the different $Fe_{42}Ni_{28}Zr_{10-x}Nb_xB_{20}$ powder blends with $x = 1, 2, 4$, and 6 at.% Nb. The arrow corresponds to the time when the amorphous phase formation has been observed.

The interesting observation made was that the 2θ value of the peak increased at the time of amorphization, i.e., lattice contraction had occurred. This observation has been made for the first time, even though this is expected to occur according to theoretical predictions. Formation of the amorphous phase during milling and the associated lattice contraction can be explained on the basis of the atomic strain model of Egami and its subsequent development by Miracle and co-workers.

Egami and Waseda[33] proposed a model to calculate the atomic strain introduced into the lattice when a solute atom of a different size is introduced into the solvent lattice and suggested that the crystalline lattice becomes destabilized once a critical strain value is exceeded. The volume mismatch was calculated from the relationship:

$$\frac{\Delta V}{V_A} = \frac{V_B - V_A}{V_A} = \left(\frac{r_B}{r_A}\right)^3 - 1, \tag{1}$$

where V and r represent the atomic volume and radius, respectively and the subscripts A and B represent the solvent and solute, respectively. Since the lattice strain was calculated to increase linearly with solute content, a minimum amount of solute was required for destabilization of the crystalline lattice. It was reported that there is a close relationship between $\frac{\Delta V}{V_A}$ and $C_B^{\min}$ according to the equation:

$$\left|\frac{V_B - V_A}{V_A}\right| C_B^{\min} = 0.1. \tag{2}$$

This concept was later extended to the case of ternary alloy systems[34] and multicomponent systems.[35] The volumetric strain due to solute addition was calculated using the relations:

$$\varepsilon_V^A = \frac{2}{3}\left(\frac{1-2\nu}{1-\nu}\right)\lambda_1, \tag{3}$$

where ε_V^A = volumetric strain, λ_1 = mismatch between solute atoms and coordination hole of the nearest neighbor atoms in the multicomponent system, ν = Poisson's ratio, and

$$\lambda_1 = \frac{\sum y_i C_i}{1 + \sum C_i (y-1)}\left[\left(\frac{2}{\sum(1+R)}\right)^3 - 1\right], \tag{4}$$

where y is a measure of the deformation required to fit the solute atom B into the hole created by the solvent atom A so that it fits into the A matrix without causing any strain in the matrix. $R = R_{\text{solute}}/R_{\text{solvent}}$ and C_i = atomic concentration of the ith element, and y is given by:

$$y = R^3\left[\frac{2}{3}\left(\frac{1-2\nu}{1-\nu}\right)\left(\frac{2}{1+R}\right)^3 + \frac{1+\nu}{3(1-\nu)}\right]. \tag{5}$$

Values of ε_V^A calculated using the above equations for the different alloys with Nb = 1, 2, 4, and 6 at.% are shown in Table 3.

It can be seen from Table 3 that the absolute value of the critical volume strain is greater than 0.054, the value above which the crystalline lattice becomes destabilized and amorphization occurs. This explains why amorphization has been achieved in all these systems. The negative values of the volumetric strain support the fact that amorphization is accompanied by a contraction of the lattice, which has been demonstrated experimentally. Calculation of the interatomic distance between the transition metal atoms (X_m in Table 3) shows that these values are high for the powder blends containing 2 and 4 at.% Nb, thus explaining the ease of destabilization of the crystalline lattice due to topological disorder. The qualitative observation that the width of the peak is larger for the 2 at.% Nb blend provides further explaination to the enhanced GFA at this composition.

Table 3. Volumetric strain and interatomic distances between transition metal (TM) atoms in the $Fe_{42}Ni_{28}Zr_{10-x}Nb_xB_{20}$ system; 2θ corresponds to the position of the broad diffuse peak at the time of amorphization and X_m is the average interatomic distance between transition metal atoms.

At.% Nb	Time for amorphization (h)	2θ (°)	X_m (nm)	Volumetric strain
1	10	44.33	0.251	−0.192
2	8	44.22	0.252	−0.191
4	10	44.10	0.252	−0.190
6	15	44.47	0.250	−0.188

The lattice contraction occurring during amorphization can also be understood in terms of the Miracle model relating the atomic diameters of the solvent and solute atoms to the coordination number. In the model of Miracle,[36,37] the solute atoms are surrounded by the solvent atoms. Depending on the atomic radii of the constituent elements, the coordination number is expected to be different. Thus, the coordination numbers are calculated to be 13, 18, 16, and 9 for Ni, Zr, Nb, and B atoms, respectively. Accordingly, the coordination number decreases from 18 to 16 when the Zr atoms are partially replaced by Nb. This results in a more efficient packing of atoms, less free volume in the matrix and leads to lattice contraction. Even though different mechanisms for glass formation have been proposed, this is perhaps the first time that clear experimental evidence is provided for some of the proposals.

3.4. *Comparison between solidification-processed and solid-state processed alloy*

Liu *et al*.[38] had earlier reported that they were able to produce the Fe-based alloy composition in a glassy state by the copper mold casting method. They were able to produce amorphous rods of $Fe_{60}Co_8Zr_{10}Mo_5W_2B_{15}$ with the dimensions of 1.5 mm in diameter and 50 mm in length. On annealing this amorphous alloy at 1023 K for 25 min, the amorphous alloy was fully crystallized to form α-Fe, $ZrFe_2$, Fe_3B, MoB_2, Mo_2FeB_2, and another unknown phase. To see if similar

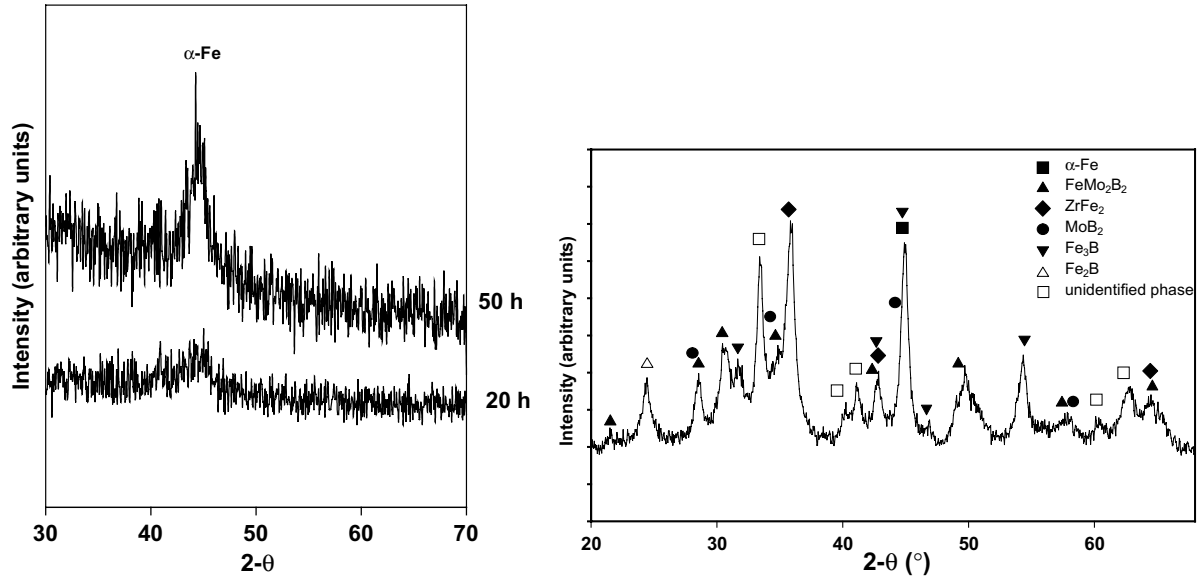

Fig. 5. (a) X-ray diffraction patterns of the $Fe_{60}Co_8Zr_{10}Mo_5W_2B_{15}$ powder blend milled for 20 and 50 h. While the powder milled for 20 h shows the presence of an amorphous phase, the powder milled for 50 h shows the presence of a crystalline phase along with an amorphous phase. This suggests that mechanical crystallization of the amorphous phase had occurred. (b) X-ray diffraction pattern of the $Fe_{60}Co_8Zr_{10}Mo_5W_2B_{15}$ amorphous powder annealed externally at 973 K for 1 h. Note that all the expected crystalline phases, and no impurity-stabilized phases, are present in the annealed powder.

results could be obtained through solid-state processing methods, we have conducted mechanical alloying experiments in a SPEX mill on blended elemental powder mixtures corresponding to the above composition. XRD experiments revealed that an amorphous phase had formed on milling the powder for 20 h. However, on continued milling of the amorphous powder, a crystalline phase started appearing. Figure 5(a) shows the XRD patterns of the $Fe_{60}Co_8Zr_{10}Mo_5W_2B_{15}$ powder mix milled for 20 h and 50 h. The powder mix milled for 20 h clearly shows the formation of an amorphous phase, indicated by the presence of a broad and diffuse halo in the XRD pattern. But, interestingly, the MA powder with a cumulative milling time of 50 h shows a sharp peak, suggesting that the amorphous phase formed earlier had started to crystallize.[39] From the position of the sharp peak, it could be deduced that it corresponds to the $(110)_{Fe}$ peak. Careful observation of the XRD patterns revealed the presence of low-intensity peaks corresponding to the other expected peaks from the α-Fe solid solution phase. Figure 5(b) shows the XRD pattern of the amorphous powder (obtained by milling for 20 h) annealed at 973 K for 1 h. From the positions and intensities of the peaks, it was determined that the annealed powder contained α-Fe, $ZrFe_2$, Fe_3B, MoB_2, Mo_2FeB_2, Fe_2B, and an unidentified phase. It is interesting to note that these phases are very similar to those obtained by solidification processing. From this experiment, it can be concluded that similar results are obtained in this alloy by both the processing methods. Similar results are also found in other alloy systems.[11,12]

4. Concluding Remarks

Amorphous phase formation has been achieved in a number of Fe-based powder mixtures by MA techniques. Based on phase diagram features, it has been suggested that the ease of amorphization increases with the number of intermetallics present in the constituent phase diagrams. This criterion is quite different from that used to explain glass formation by RSP methods. Mechanical crystallization of the amorphous phase on continued milling of the amorphous powder and lattice contraction during amorphization are novel features to MA. While mechanical crystallization provides an opportunity to design alloys with different microstructures, the phenomenon of lattice contraction helps in understanding the atomistic mechanism of amorphization during MA. These observations clearly bring out the important fact that glass formation by RSP and MA methods is quite different. However, the greatest advantage of MA will be in the synthesis of BMG alloys. This is because once the powder is produced in the amorphous state, it could be consolidated in the supercooled liquid region to any section thickness. Thus, the properties of the liquid, which define the GFA of alloys by solidification methods, will not be a limitation in alloys processed by MA.

References

1. C. Suryanarayana, *Bull. Mater. Sci.* **6**, 579 (1984).
2. T. R. Anantharaman (ed.), *Metallic Glasses: Production, Properties and Applications*, Trans Tech Publications, Aedermannsdorf, Switzerland (1984).

3. H. H. Liebermann (ed.), *Rapidly Solidified Alloys: Processes, Structures, Properties, Applications* (Marcel Dekker, New York, 1993).
4. W. Klement, R. H. Willens and P. Duwez, *Nature (London)* **187**, 869 (1960).
5. A. Inoue, *Acta Mater.* **48**, 279 (2000).
6. W. L. Johnson, *MRS Bull.* **24**(10), 42 (1999).
7. M. K. Miller and P. K. Liaw (ed.), *Bulk Metallic Glasses*, (Springer, New York, 2008).
8. C. Suryanarayana and A. Inoue, *Bulk Metallic Glasses*, (CRC Press/Taylor & Francis, Boca Raton, FL, 2010).
9. Z. P. Lu and C. T. Liu, *Acta Mater.* **50**, 3501 (2002).
10. C. Suryanarayana, I. Seki and A. Inoue, *J. Non-Cryst. Solids* **355**, 355 (2009).
11. C. Suryanarayana, *Prog. Mater. Sci.* **46**, 1 (2001).
12. C. Suryanarayana, *Mechanical Alloying and Milling*, (Marcel Dekker, New York, 2004).
13. M. Sherif El-Eskandarani and A. Inoue, *J. Mater. Res.* **21**, 976 (2006).
14. C. Suryanarayana and M. G. Norton, *X-Ray Diffraction: A Practical Approach*, (Plenum Press, New York, 1998).
15. E. Ma, *Prog. Mater. Sci.* **50**, 413 (2006).
16. S. Sharma, C. Suryanarayana and R. Vaidyanathan, *Appl. Phys. Lett.* **90**, 086108 (2007).
17. S. Sharma and C. Suryanarayana, *J. Appl. Phys.* **102**, 083544 (2007).
18. T. B. Massalski, *Binary Alloy Phase Diagrams*, ASM International, Material Park, OH (1990).
19. Y. S. Cho and C. C. Koch, *J. Alloys Compd.* **194**, 287 (1993).
20. F. H. Froes, C. Suryanarayana, K. C. Russell and C. G. Li, *Mater. Sci. Eng. A* **192/193**, 612 (1995).
21. T. Klassen, M. Oehring and R. Bormann, *Acta Mater.* **45**, 3935 (1997).
22. N. S. Stoloff and R. G. Davies, *Prog. Mater. Sci.* **13**, 77 (1966).
23. D. Turnbull, *Contemp. Phys.* **10**, 473 (1969).
24. R. Wong and M. D. Merz, *Nature (London)* **260**, 35 (1976).
25. U. M. R. Seelam and C. Suryanarayana, University of Central Florida, Orlando, FL, USA, Unpublished results (2006).
26. M. Nose and T. Masumoto, *Sci. Rep. Res. Inst. Tohoku Univ.* **A28**, 135 (1980).
27. U. Köster and U. Herold, In: H. J. Güntherodt and H. Beck (eds.), *Glassy Metals I*, (Springer-Verlag, Berlin, 1981), p. 225.
28. M. L. Trudeau, R. Schulz, D. Dussault and A. Van Neste, *Phys. Rev. Lett.* **64**, 99 (1990).
29. C. Suryanarayana, *Intermetallics* **3**, 153 (1995).
30. A. Blatter and M. Von Allmen, *Phys. Rev. Lett.* **54**, 2103 (1985).
31. E. S. Park and D. H. Kim, *Acta Mater.* **54**, 2597 (2006).
32. A. R. Miedema, F. R. de Boer and R. Boom, *CALPHAD* **1**, 341 (1997).
33. T. Egami and Y. Waseda, *J. Non-Cryst. Solids* **64**, 113 (1984).
34. Z. J. Yan, J. F. Li, S. R. He and Y. H. Zhou, *Mater. Res. Bull.* **38**, 681 (2003).
35. T. Egami, *J. Non-Cryst. Solids* **317**, 30 (2003).
36. D. B. Miracle, *Nature Mater.* **3**, 697 (2004).
37. D. B. Miracle, *Acta Mater.* **54**, 4317 (2006).
38. D. Y. Liu, W. S. Sun, A. M. Wang, H. F. Zhang and Z. Q. Hu, *J. Alloys Compd.* **370**, 249 (2004).
39. U. Patil, S. J. Hong and C. Suryanarayana, *J. Alloy. Compd.* **389**, 121 (2005).